AD-A147 881 REMOTE SENSING OF THE HIGH LATITUDE IONOSPHERE(U) 1/1
AEROSPACE CORP EL SEGUNDO CA SPACE SCIENCES LAB
P F MIZERA ET AL. 01 AUG 84 TR-0084(4478-32)-1
UNCLASSIFIED SD-TR-84-30 F04701-83-C-0084 F/G 4/2 NL

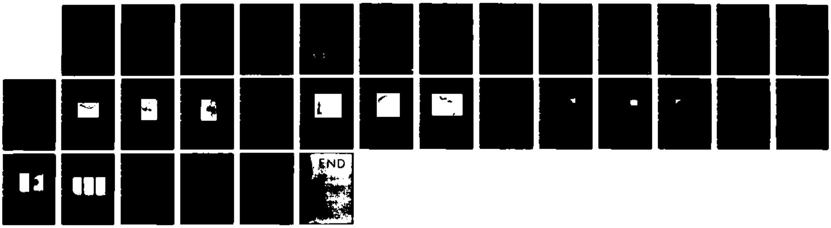

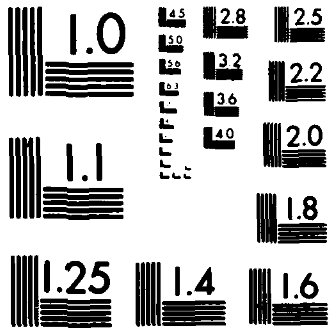

MICROCOPY RESOLUTION TEST CHART
NATIONAL BUREAU OF STANDARDS 1963 A

REPORT SD-TR-84-30

(12)

AD-A147 881

Remote Sensing of the High Latitude Ionosphere

P. F. MIZERA and D. J. GORNEY
Space Sciences Laboratory
Laboratory Operations
The Aerospace Corporation
El Segundo, Calif. 90245

1 August 1984

APPROVED FOR PUBLIC release;
DISTRIBUTION UNLIMITED

Prepared for

SPACE DIVISION
AIR FORCE SYSTEMS COMMAND
Los Angeles Air Force Station
P.O. Box 92960, Worldway Postal Center
Los Angeles, Calif. 90009

84 11 08 013

This report was submitted by The Aerospace Corporation, El Segundo, CA 90245, under Contract No. F04701-83-C-0084 with the Space Division, P.O. Box 92960, Worldway Postal Center, Los Angeles, CA 90009. It was reviewed and approved for The Aerospace Corporation by H. R. Rugge, Director, Space Sciences Laboratory. First Lt Douglas R. Case, SD/YCM, was the Project Officer.

This report has been reviewed by the Public Affairs Office (PAS) and is releasable to the National Technical Information Service (NTIS). At NTIS, it will be available to the general public, including foreign nationals.

This technical report has been reviewed and is approved for publication. Publication of this report does not constitute Air Force approval of the report's findings or conclusions. It is published only for the exchange and stimulation of ideas.

Douglas R. Case, 1st Lt, USAF
Project Officer

Joseph Hess, GM-15, Director, West Coast Office, AF Space Technology Center

UNCLASSIFIED

SECURITY CLASSIFICATION OF THIS PAGE (When Data Entered)

REPORT DOCUMENTATION PAGE

READ INSTRUCTIONS BEFORE COMPLETING FORM

1. REPORT NUMBER: SD-TR-84-30	2. GOVT ACCESSION NO.: A147881
3. RECIPIENT'S CATALOG NUMBER	
4. TITLE (and Subtitle): REMOTE SENSING OF THE HIGH LATITUDE IONOSPHERE	5. TYPE OF REPORT & PERIOD COVERED
	6. PERFORMING ORG. REPORT NUMBER: TR-0084(4478-32)-1
7. AUTHOR(s): Paul F. Mizera and David J. Gorney	8. CONTRACT OR GRANT NUMBER(s): F04701-83-C-0084
9. PERFORMING ORGANIZATION NAME AND ADDRESS: The Aerospace Corporation, El Segundo, Calif. 90245	10. PROGRAM ELEMENT, PROJECT, TASK AREA & WORK UNIT NUMBERS
11. CONTROLLING OFFICE NAME AND ADDRESS: Space Division, Air Force Systems Command, Los Angeles, Calif. 90009	12. REPORT DATE: 1 August 1984
	13. NUMBER OF PAGES: 30
14. MONITORING AGENCY NAME & ADDRESS (if different from Controlling Office)	15. SECURITY CLASS. (of this report): Unclassified
	15a. DECLASSIFICATION/DOWNGRADING SCHEDULE

16. DISTRIBUTION STATEMENT (of this Report)

Approved for public release; distribution unlimited.

17. DISTRIBUTION STATEMENT (of the abstract entered in Block 20, if different from Report)

18. SUPPLEMENTARY NOTES

19. KEY WORDS (Continue on reverse side if necessary and identify by block number)

Auroral
Density Perturbations
High Latitude Ionosphere
Remote Sensing
UV
Visible
X-rays

20. ABSTRACT (Continue on reverse side if necessary and identify by block number)

Remote sensing of the earth's ionosphere has many applications to radio wave communications. Techniques to monitor perturbations of the quiescent ionosphere at high latitudes from satellites are described, which include observations in the visible, ultra-violet and X-ray wavelengths.

DD FORM 1473 (FACSIMILE)

UNCLASSIFIED

SECURITY CLASSIFICATION OF THIS PAGE (When Data Entered)

PREFACE

The following reference was used extensively in the Introduction: Goodman, John M. and Jules Aarons, The Radiowave Propagation Environment - Science and Technology Objectives for the 80's, Effect of the Ionosphere on Radiowave Systems, NRL and AFGL 1981.

CONTENTS

FIGURES

FIGURES (Continued)

TABLE

Introduction

The earth is surrounded by a cold ionized plasma called the ionosphere, which has been a topic of considerable scientific study ever since the advent of radio communications. The ionization of neutral atmospheric constituents is due primarily to the action of the sun's radiation beyond 100 km above the surface of the earth. The lowest region of the ionosphere is called the D region whose upper boundary is around 90 km altitude. This region is an absorbing medium due to the high frequency of electron collisions. Ionization in the D region is caused by weakly absorbed radiation such as precipitating energetic particles, hard solar radiation (0.1 to 1.0 nm; 1.0 nm ≈ 1.2 keV), Lyman α emissions from hydrogen and longer wavelength radiation that only ionizes excited air molecules. Electromagnetic radiation is highly absorbed when electron concentrations are large. These conditions exist during periods of intense solar activity such as solar flares and polar cap absorption (PCA) events.

The E region lies above the D region and extends to approximately 150 km altitude. Next is the F region where the maximum electron concentration usually occurs near the F_2 peak at ≈ 250 km.

Photoionization by solar radiation is the primary mechanism for ionizing high altitude atmospheric gases. However, precipitation by charged particles at high latitudes can have significant effects on the properties of the ionosphere.

The ionosphere is not a static medium. The neutral atmosphere is in a state of continuous motion which interacts with the ionized plasma in different ways depending on the altitude. In the D region below 90 km, collisions between ionized and neutral gases are frequent enough to make the plasma velocity essentially equal to the neutral gas. In the E and F regions between 90 and 250 km altitude, the earth's magnetic field controls ion and electron motion influenced by neutral gas motion. Above the F_2 peak, the neutral density becomes so small that collisions become less important and usual hydromagnetic forces prevail.

In the altitude region between 90 and 200 km, ionized plasma can move relative to the neutral atmosphere causing currents to flow. The generation of these current systems is further complicated by temporal and spatial variations of E-region conductivity and the requirement for closure of the global current system.

Table 1 summarizes changes in the ionosphere that affect different bandwidths of radio communications. Irregularities in the ionosphere can result from solar induced phenomena including the aurora. Changes in the E-region conductivity are an important aspect of this presentation.

Global Imaging

A remote sensing capability of E-region ionization is necessary to understand global current systems. Ionosondes and topside sounders are tools that directly measure ionization enhancements by observing reflected radio signals. These techniques are not easily adaptable for remote sensing. However, electromagnetic radiation emitted in the process of ionization can be monitored on a global scale from a satellite platform. Figure 1 shows a schematic representation of the earth's ionosphere before and after a solar disturbance. Inputs to the ionosphere directly from the sun and indirectly through the magnetosphere can be imaged in the visible, ultraviolet and X-ray

Table 1 Radiowave propagation deficiencies

Type	Frequency	Application	Deficiency
ELF	30-300 Hz	One way communication with submerged submarines	Upper boundary of the propagation wave guide is susceptible to large scale irregularities
VLF	3-30 kHz	VLF navigation and communication	Degrading effects on communication due to changes in signal attenuation, phase and phase rate attributed to perturbation in the propagating medium
MF/HF	0.3-30 MHz	Principal element in the Navy communications system and over-the-horizon radar	HF band sensitive to ionospheric variations due to solar disturbbances
UHF/SHF	0.3-30 GHz	Beyond line of sight communications	Scintillation due to ionospheric irregularities especially at F region altitude

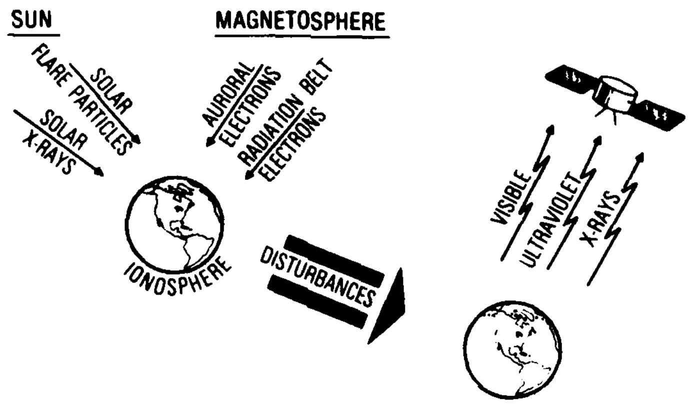

Fig. 1 The earth's ionosphere receives disturbances from the sun and the magnetosphere which can be imaged by satellite instruments.

wavelengths by satellite instrumentation. Historically the methods used can be categorized by wavelength bands.

Visible Imaging

The first scientific satellite to fly a visible imager was the Canadian ISIS-2. Scanning photometers centered on atomic oxygen emissions at 630.0 and 557.7 nm and molecular nitrogen at 391.4 nm were used to image auroral arcs at altitudes near 2000 km, high enough to image the entire polar region under ideal sun conditions (Anger et al.).[1] Some of the results of that program are summarized by Murphree et al.[2]

Early in the 1970's, the USAF DMSP satellites began photographing auroral arcs with good spatial resolution over a broad wavelength band towards the infrared (Eather).[3] Figure 2 and Figure 3 show two composites of DMSP auroral imagery taken over Europe and the North American continent during winter months when the polar regions are dark. The composite images are three consecutive orbits at the same local time but over different regions of the earth. The distance across each photograph at the auroral altitude is approximately 2300 km. Figures 2 and 3 show how polar orbiting satellites can image the ionization in the E and F regions of the ionosphere.

Figure 4 is a single orbit image over the south pole during the northern summer and illustrates the variability and the dynamic nature of the particle precipitation responsible for changes in the E and F region conductivities.

UV Imaging

The visible images shown in the previous section were obtained by satellite instruments during ideal viewing conditions. Most of the time, the

Fig. 2 Visible images of the northern auroral lights superimposed on a DMSP image of Europe taken at night.

Fig. 3 Visible images of the northern auroral lights superimposed on a DMSP image of the United States taken at night.

Fig. 4 An unusual image of the aurora taken over the South Pole with midnight at the top and dusk to the left.

polar regions of the earth are partially illuminated by sunlight and during solstice periods, one pole is almost completely sunlit. Some ultra-violet emissions can be selected to reduce the amount of scattered sunlight penetrating the atmosphere into a satellite imager (Meng et al.).[4] An example of imaging a portion of the aurora by a low altitude polar orbiting satellite called Hilat is shown in Figure 5. The image is taken at 149.3 nm in full sunlight.

An imager flown on the Dynamics Explorer (DE-1) satellite at altitudes up to 4 Re has provided full earth images in both UV and visible wavelengths. Figure 6 shows the northern polar region on November 8, 1981 from an altitude near 20,000 km. The image was taken in the 123.0 to 165.0 nm UV wavelength bands. These auroral emissions arise primarily from the 130.4 and 135.6 nm atomic oxygen lines.

X-Ray Imaging

At wavelengths down to 0.1-1 nm, the auroral emissions arise primarily from the bremsstrahlung process. Instead of the precipitating electrons exciting atmospheric atoms and molecules, they can lose some of their energy in the form of X-rays. The production of these X-rays is nearly independent of atmospheric species. Measurements taken at the longer wavelengths are usually limited to one or two emissions and are usually of a single atmospheric species. The shape of the bremsstrahlung X-ray spectrum is more directly related to the input electron spectrum and is not strongly dependent on atmospheric composition.

The first auroral X-ray measurements taken from a polar orbiting satellite were made by the DMSP-F2 which was launched in 1977. Figure 7 shows

Fig. 5 A portion of the auroral region imaged at 149.3 nm (Lyman-Birge-Hopfield bands of N_2) in full sunlight. A narrow arc is seen crossing the southern part of Greenland at the bottom left corner on July 23, 1983 by the AFGL/APL instrument aboard the Hilat satellite (Courtesy of C. Meng).

Fig. 6 A full view of the earth's northern polar region imaged in the 123.0 to 165.0 nm wavelength band. Local midnight is at the bottom right of the auroral oval. The earth's terminator crosses the equatorward boundary of the local moon aurora. The image was taken by the University of Iowa instrument aboard the Dynamics Explorer-1 satellite (Courtesy of L. Frank and J. Craven).

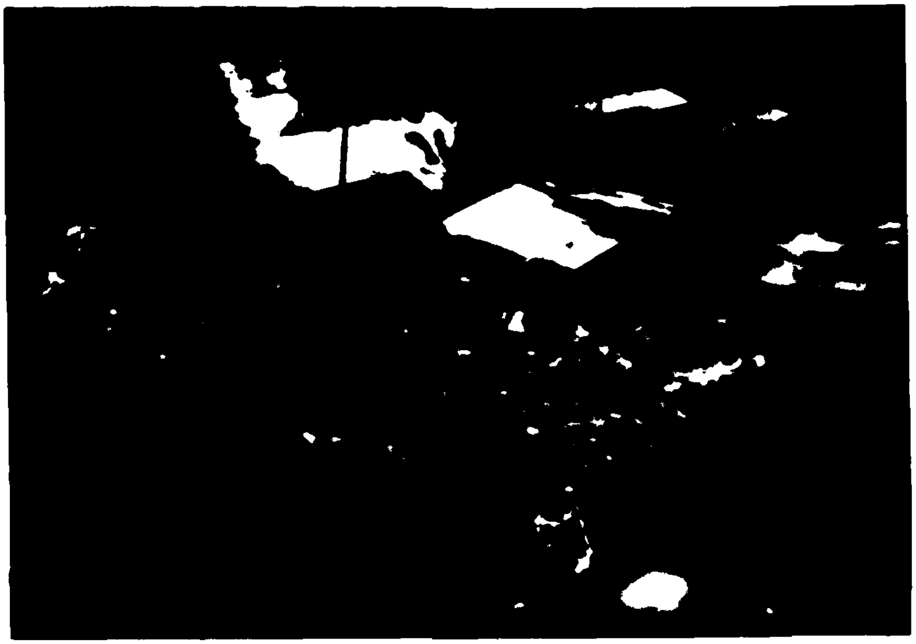

Fig. 7 Three auroral crossings of the North American continent showing city lights, auroral light and bremsstrahlung X-ray fluxes from 1.5 to 20 keV along the vertical scale. The X-ray energy flux intensity is shown as vertical lines as the satellite crosses over the auroral arcs. These data were taken with The Aerospace Corporation X-ray spectrometer flown aboard the DMSP-F2 satellite on December 2, 1977.

the same composite of city lights and visible auroral as in Figure 3 with X-ray intensities superimposed on the auroral light. The vertical scale covers energies from 1.5 to 20 keV in 15 integral steps and the X-ray flux intensity is depicted by the shades of gray in the vertical lines.

Various methods have been examined by us to invert the bremsstrahlung process formalism in order to determine the input electron spectrum. Once a satisfactory electron spectrum is derived then standard calculations can produce energy input rates, ionization densities and conductivities.

Figure 8 shows a dawn (a) and a dusk (b) crossing of the northern auroral regions on January 31, 1978. The aurora are barely visible in the photographs probably due to sunlight contamination. The three-dimensional plots are height profiles of the energy density deposition rates as a function of time or crossing of the polar regions. In each case, the top curve represents calculations of the average electron energy deposition (keV/cm^3 - sec) from the directly measured precipitation electron from 1 to 20 keV. The bottom curve, marked "X-Rays", represents calculations using the inferred or inverted electron spectra. The inversion technique has been discussed by Brown[5] and presented by Mizera and Gorney.[6] The energy deposition rates calculated from both the directly measured electron spectrum and the X-ray spectrum are in very good agreement.

Figure 9 shows electron density (cm^{-3}) as a function of altitude for the January 31 auroral crossings shown in Figure 8. The solid (dashed) line represents the maximum energy deposition rate for the dawn (dusk) electron precipitation. The Δ (O) represents the same calculation using the electron spectrum calculated from the X-rays.

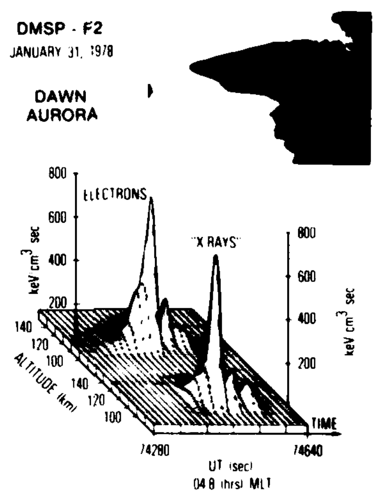

Fig. 8a A dawn photograph of the northern auroral region with midnight on the top right taken on January 31, 1978 by the DMSP-F2 satellite. The 3-D plots are energy deposition rates calculated from precipitating electrons from 1-20 keV (top) and from X-ray fluxes. The altitude profiles extend from 150 km down to 80 km. The satellite crosses the auroral arc near 4.8 hrs. magnetic local time.

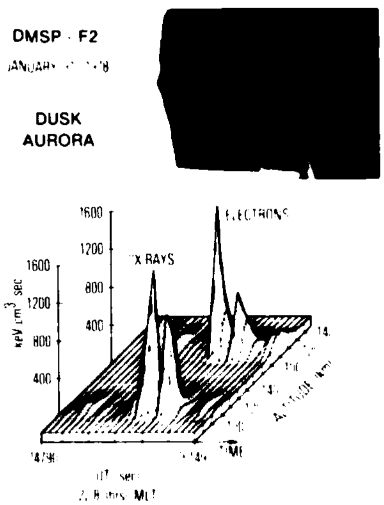

Fig. 8b The dusk continuation of the January 31, 1978 northern auroral crossing. Visible auroral arcs are seen at the bottom of the photograph and extend under the satellite ground track. Even though the auroral arcs are barely visible, the energy deposition rates are almost a factor of 2 larger than the dawn crossing.

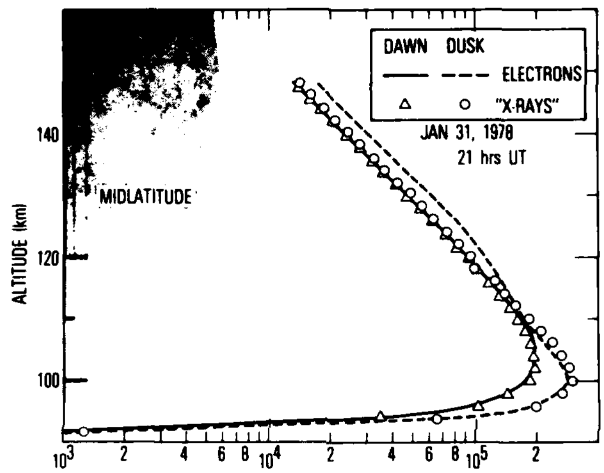

Fig. 9 Altitude profiles of the logarithm of the electron density (cm^{-3}) calculated from the peak dawn and dusk energy depositions on January 31, 1978 (Figs. 8a and b). Note how the dusk local time electron density is almost a factor of 2 larger than the dawn and occurs at a lower altitude.

Once the electron density is determined, standard conductivity calculations can be made. Figure 10 shows the height profiles and integrated Pedersen and Hall conductivities calculated from the electron density in the dawn (a) and the dusk (b) profiles. From this example and numerous others, we can obtain reasonably accurate representations of the primary electron spectrum by remotely sensing auroral X-ray fluxes and thus infer the perturbations in the ionospheric density.

The first limb to limb X-ray images of the high latitude regions of the earth were obtained by a scanning imager flown on the DMSP-F6 satellite launched into a dawn-dusk local time orbit on December 20, 1982. Figure 11 shows two images taken on January 18, 1983. The image on the right shows the standard USAF DMSP visible image and that on the left was taken in the X-ray energy range from 2 to 21 keV. The visible image has spatial resolution of a few km whereas the X-ray image has spatial resolution of 100 km. Nevertheless, the macroscopic features of the visible aurora such as dawn and dusk boundaries, the surge of electron precipitation onto the polar cap are well duplicated in the X-ray image.

Figure 12 shows three consecutive X-ray images of the earth's polar regions with the north polar crossing, shown in the previous figure, displayed in the middle panel. The two south polar crossings, preceding and following the north polar crossing, are displayed on the left and right, respectively. The southern images have been reversed in time so that the dawn auroral crossings are on the bottom, local midnight is to the left and the dusk aurora are on top in order to correspond with the north polar crossing format. Figure 12 clearly shows that scattered X-rays from the sunlit southern polar cap do not degrade the X-ray image.

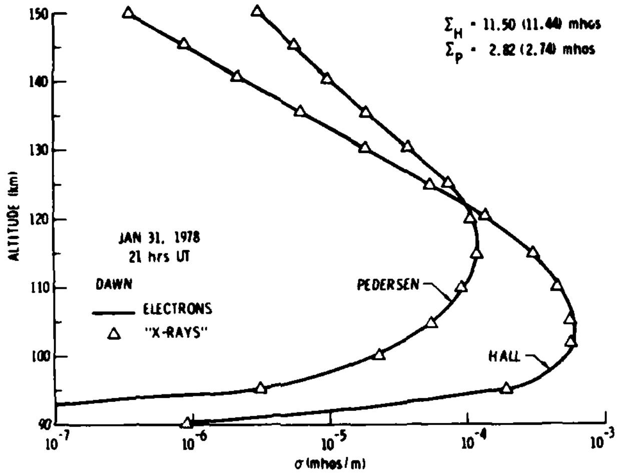

Fig. 10a The dawn altitude profiles of the Pedersen and Hall conductivities in (mhos/m) for the peak electron density shown in Fig. 9. The height integrated conductivities are also shown with those calculated from the X-ray measurement in parenthesis.

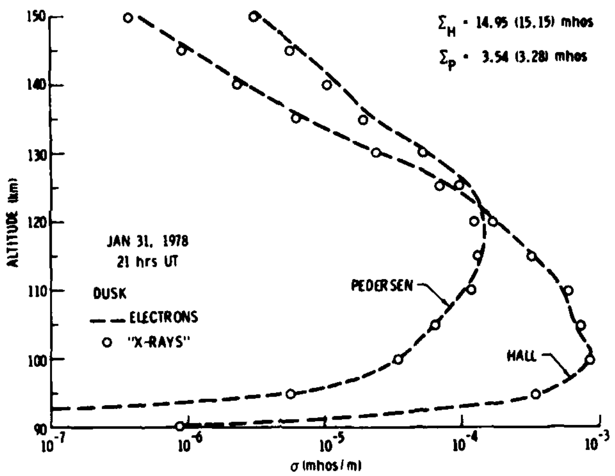

Fig. 10b Same as Fig. 10a but for the peak electron profile in the dusk shown in Fig. 9.

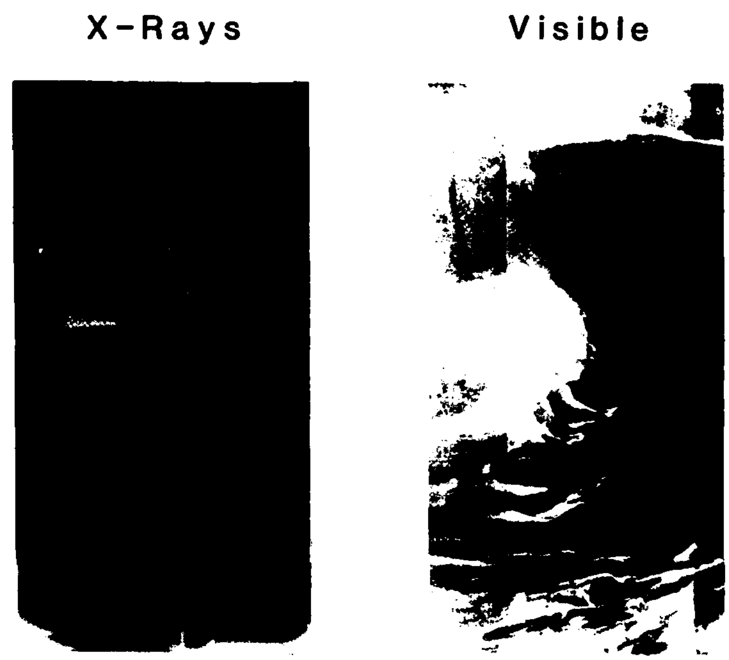

Fig. 11 X-ray and visible images taken by instruments aboard the DMSP-F6 satellite on January 18, 1983. The X-ray image was obtained by The Aerospace Corporation's scanning X-ray spectrometer. Black is background and white is maximum X-ray intensity from 2 to 20 keV. Note how the most intense electron energy deposition occurs in the middle of the polar auroral vortex. Dawn is at the bottom and midnight is on the left.

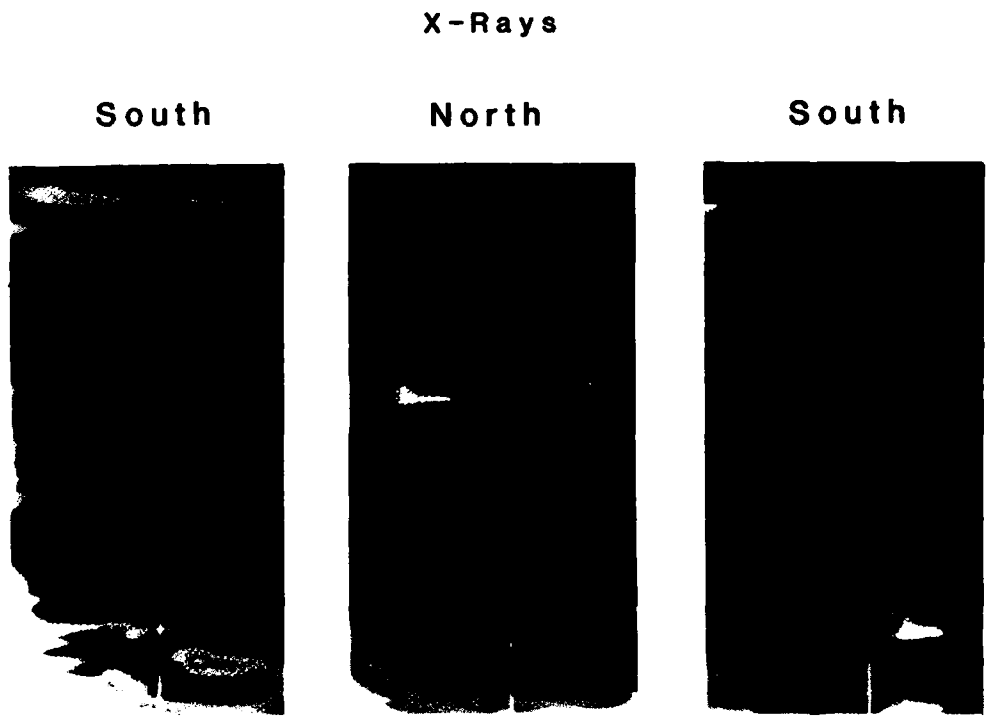

Fig. 12 Three consecutive X-ray images taken on January 18, 1983. The two outer images were taken over the sunlit southern polar region with no increase in signal background.

Summary

The ionosphere plays an important role in communications of radio waves from very low frequencies in the ELF range to ultra high frequencies in the UHF range. The ionosphere is also an important boundary between atmospheric and magnetospheric phenomena. Enhanced ionization and conductivity changes are important quantities that should be monitored on a global scale in near real time. Precipitating electrons above a few keV are a major source of high latitude ionospheric perturbations. Determining the magnitude of this source requires remote sensing of electromagnetic radiation emitted as a by-product of the ionization.

In the visible wavelengths, light is emitted from different excited states of atoms and molecules at different altitudes. Some information about the height dependence of the ionization can be obtained by comparing different wavelength emissions. Also, a commonly observed emission at 391.4 nm from molecular nitrogen is thought to vary in proportion to the total energy deposited where nitrogen is abundant.

UV imaging has some advantages over visible in its ability to observe certain UV wavelength emissions in the presence of scattered sunlight. However quantitative information about the altitude and intensity of ionization is not yet available.

X-rays in the keV energy range can be used to image the source of ionization in daylight and darkness and provide information about the primary electron spectrum. As X-ray imagers become more sophisticated, the temporal and spatial resolution of the images will improve.

References

1. Anger, C. D., A. T. Y. Lui and S. -I. Akasofu, Observations of the Auroral Oval and a Westward Traveling Surge from the ISIS-2 Satellite and the Alaskan Meridian All-Sky Cameras, J. Geophys. Res., 78, 3020, 1973.

2. Murphree, J. S., C. D. Anger and L. L. Cogger, ISIS-2 Observations of Auroral Arc Systems, Physics of Auroral Arc Formation, Geophys. Monograph, 25, 15, S. -I. Akasofu and J. R. Kan, eds., AGU Washington, D. C., 1981.

3. Eather, R. H., DMSP Calibration, J. Geophys. Res., 84, 4134, 1979.

4. Meng, C. -I., R. R. Babcock and R. E. Huffman, Ultraviolet Imaging for Auroral Zone Remote Sensing, AIAA-83-0019, 21st ASM, January 10-13, 1983, Reno, Nevada.

5. Brown, J. C., The Deduction of Energy Spectra of Nonthermal Electrons in Flares from the Observed Dynamic Spectra of Hard X-Ray Bursts, Sol. Phys., 18, 489, 1971.

6. Mizera, P. F. and D. J. Gorney, X-Rays from the Aurora, Proc. European Geophysical Society, Polar Aurora Symposium, Leeds, England, 1982.

U S GOVERNMENT PRINTING OFFICE 1984 584 070

LABORATORY OPERATIONS

The Laboratory Operations of The Aerospace Corporation is conducting experimental and theoretical investigations necessary for the evaluation and application of scientific advances to new military space systems. Versatility and flexibility have been developed to a high degree by the laboratory personnel in dealing with the many problems encountered in the nation's rapidly developing space systems. Expertise in the latest scientific developments is vital to the accomplishment of tasks related to these problems. The laboratories that contribute to this research are:

Aerophysics Laboratory: Launch vehicle and reentry aerodynamics and heat transfer, propulsion chemistry and fluid mechanics, structural mechanics, flight dynamics; high-temperature thermomechanics, gas kinetics and radiation; research in environmental chemistry and contamination; cw and pulsed chemical laser development including chemical kinetics, spectroscopy, optical resonators and beam pointing, atmospheric propagation, laser effects and countermeasures.

Chemistry and Physics Laboratory: Atmospheric chemical reactions, atmospheric optics, light scattering, state-specific chemical reactions and radiation transport in rocket plumes, applied laser spectroscopy, laser chemistry, battery electrochemistry, space vacuum and radiation effects on materials, lubrication and surface phenomena, thermionic emission, photosensitive materials and detectors, atomic frequency standards, and bioenvironmental research and monitoring.

Electronics Research Laboratory: Microelectronics, GaAs low-noise and power devices, semiconductor lasers, electromagnetic and optical propagation phenomena, quantum electronics, laser communications, lidar, and electro-optics; communication sciences, applied electronics, semiconductor crystal and device physics, radiometric imaging; millimeter-wave and microwave technology.

Information Sciences Research Office: Program verification, program translation, performance-sensitive system design, distributed architectures for spaceborne computers, fault-tolerant computer systems, artificial intelligence, and microelectronics applications.

Materials Sciences Laboratory: Development of new materials: metal matrix composites, polymers, and new forms of carbon; component failure analysis and reliability; fracture mechanics and stress corrosion; evaluation of materials in space environment; materials performance in space transportation systems; analysis of systems vulnerability and survivability in enemy-induced environments.

Space Sciences Laboratory: Atmospheric and ionospheric physics, radiation from the atmosphere, density and composition of the upper atmosphere, aurorae and airglow; magnetospheric physics, cosmic rays, generation and propagation of plasma waves in the magnetosphere; solar physics, infrared astronomy; the effects of nuclear explosions, magnetic storms, and solar activity on the earth's atmosphere, ionosphere, and magnetosphere; the effects of optical, electromagnetic, and particulate radiations in space on space systems.